# Generalized Cahn-Hilliard equation for biological applications

Evgeniy Khain[1] and Leonard M. Sander[2]
[1]*Department of Physics, Oakland University, Rochester, Michigan 48309, USA*
[2]*Department of Physics and Michigan Center for Theoretical Physics, The University of Michigan, Ann Arbor, Michigan 48109, USA*
(Received 14 January 2008; published 28 May 2008)

Recently we considered a stochastic discrete model which describes fronts of cells invading a wound [E. Khain, L. M. Sander, and C. M. Schneider-Mizell, J. Stat. Phys. **128**, 209 (2007)]. In the model cells can move, proliferate, and experience cell-cell adhesion. In this work we focus on a continuum description of this phenomenon by means of a generalized Cahn-Hilliard equation (GCH) with a proliferation term. As in the discrete model, there are two interesting regimes. For subcritical adhesion, there are propagating "pulled" fronts, similar to those of the Fisher-Kolmogorov equation. The problem of front velocity selection is examined, and our theoretical predictions are in the good agreement with a numerical solution of the GCH equation. For supercritical adhesion, there is a nontrivial transient behavior, where density profile exhibits a secondary peak. To analyze this regime, we investigated relaxation dynamics for the Cahn-Hilliard equation without proliferation. We found that the relaxation process exhibits self-similar behavior. The results of continuum and discrete models are in good agreement with each other for the different regimes we analyzed.

DOI: 10.1103/PhysRevE.77.051129 PACS number(s): 05.70.Ln, 05.45.−a, 87.18.Hf, 05.50.+q

## I. INTRODUCTION

In this paper we propose a continuum method for dealing with cells that move, proliferate, and interact via adhesion. This problem arises in models for wound healing [2] and tumor growth [3]. It is easy to formulate a discrete model for these processes [1]. However, proceeding to the continuum limit is nontrivial [4].

Consider first a simple discrete model for diffusion and proliferation. Each lattice site can be empty or once occupied. At each time step, a particle is picked at random. Then it can either jump to a neighboring empty site, or proliferate there (a new particle is born). We can try to formulate a continuum analog of this model. It was shown [5–7] that for *small* proliferation rates the propagating fronts in this discrete system can be described by the Fisher-Kolmogorov (FK) equation [8]

$$\frac{\partial u}{\partial t} = \bar{D}\frac{\partial^2 u}{\partial x^2} + \alpha u(1-u), \tag{1}$$

where $u$ is the (local) cell density, $\bar{D}$ is the cell diffusion coefficient, and $\alpha$ is the rate of proliferation [9]. Equation (1) admits solutions in a form of propagating fronts, but the velocity selection is a nontrivial problem. There is a range of possible velocities; initially sufficiently localized density profiles develop into propagating fronts with the "critical" velocity $v=2\sqrt{\bar{D}\alpha}$ [10].

Next, consider a discrete model which includes diffusion and cell-cell adhesion, but not proliferation. When a particle is picked at random, the probability to jump decreases with the number of nearest neighbors, taking into account cell-cell adhesion [1]. This scheme can be mapped into the Ising model [11,12] by identifying an empty site with spin down, and an occupied site with spin up. There is a simple relation between the average density $u$ and the average magnetization $m$ in the Ising model: $u=(m+1)/2$. The number of particles is fixed because there is no proliferation, and there are nearest-neighbor interactions between particles. Above the critical strength of cell-cell adhesion (or below a critical temperature in the Ising model), the homogeneous state becomes unstable, which leads to phase separation between high density clusters and a dilute gas of particles. The dynamics of phase separation and coarsening (where larger clusters grow at the expense of smaller ones) is usually described by the Cahn-Hilliard equation [13]; a version of this equation can be derived directly from the microscopic model [14].

We can easily add proliferation to this lattice model [1], so that we have diffusion, proliferation, and cell-cell adhesion. In this paper we suggest that the proper candidate for a continuum description is a Cahn-Hilliard equation with a proliferation term added, the GCH equation.

The rest of the paper is organized as follows. In Sec. II we present both discrete and continuum models which include diffusion, proliferation, and cell-cell adhesion and present a general phase diagram. Section III describes the front propagation problem for subcritical adhesion. Section IV focuses on a supercritical adhesion both for zero and nonzero proliferation. Section V includes a brief discussion and summary of our results.

## II. DISCRETE AND CONTINUUM MODELS

### A. Discrete model

We review the discrete model for diffusion, proliferation, and cell-cell adhesion [1]. Consider a square two-dimensional lattice in channel geometry. The lattice distance is assumed to be equal to the cell diameter, taking into account hard-core exclusion. Initially, we put cells into the left part of the channel. We take $x$ to measure the distance along the channel. A cell is picked at random, and one of the four neighboring sites is also picked at random. If this site is empty, the cell can proliferate to this site (so that a new cell is born there), or migrate there. We denote the probability for proliferation by $\alpha$. Cell-cell adhesion is represented by a

 

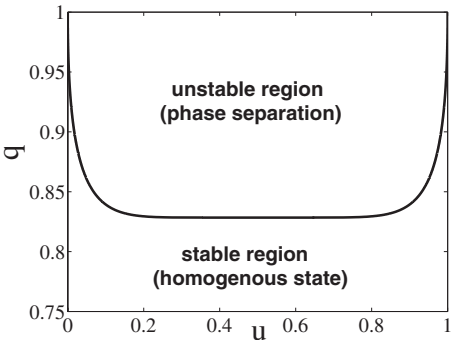


FIG. 1. Phase diagram without proliferation. The critical adhesion parameter as a function of density as given by Eq. (2) is shown by a solid line. This curve separates two qualitatively different regions. In the stable region, a homogeneous state (with uniformly distributed cells) remains homogeneous; in contrast, in the unstable region phase separation occurs and large clusters are formed.

probability for migration that decreases with the number of nearest neighbors: $p_{migr}=(1-\alpha)(1-q)^n$, where $0\leq q<1$ is the adhesion parameter, and $1\leq n\leq 4$ is the number of nearest neighbors. The case $q=0$ means no adhesion and reduces to the model of Refs. [5–7]. For nonzero $q$, it is much harder for a cell to diffuse if it has many neighbors. After each step, time is advanced by $1/N$, where $N$ is the current number of cells.

*Without* proliferation the model can be mapped into the Ising model, as we pointed out in [1]. In this mapping the adhesion parameter $q$ is identified with $1-\exp(-J/k_BT)$, where $T$ is the temperature, $k_B$ is Boltzmann's constant, and $J$ is the coupling strength in the magnetic model, and the average density $u$ is identified with $(m+1)/2$, where $m$ is the average magnetization. The mapping is possible because our dynamical rules satisfy detailed balance. Therefore, the statics of our model is the same as in the Ising model. By statics, we mean a phase diagram $(m,T)$ [or $(u,q)$ in our case] which has stable and unstable regions. In the stable region, a homogeneous state (with uniformly distributed cells) remains homogeneous; in contrast, in the unstable region, phase separation occurs and large clusters are formed.

The two-dimensional Ising model was solved by Onsager [11], and the curve $m(T)$, which separates the stable and unstable regions, is known (see Fig. 1). In our case the threshold is given by the critical adhesion parameter $q_c$ as a function of average density $u$ as follows:

$$u=\frac{1}{2}\pm\frac{1}{2}\left[1-\frac{16(1-q_c)^2}{q_c^4}\right]^{1/8}. \tag{2}$$

The unstable region corresponds to $q>q_c$, so for supercritical adhesion there is a phase separation and large clusters are formed. Interestingly, even if we start with $q<q_c$, the initially homogeneous state can become unstable when one turns on proliferation, which leads to phase separation and clustering.

### B. Continuum approach

To describe the coarse-grained dynamics of the discrete model, we take a continuum approach. A model equation,

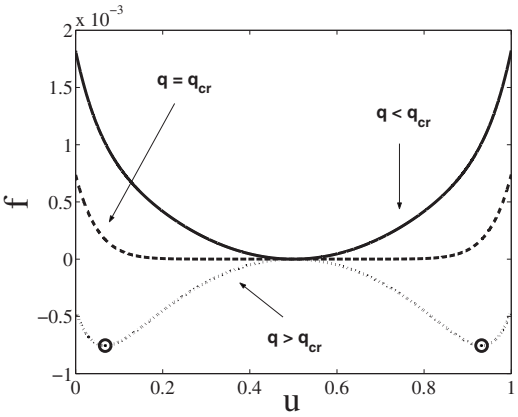


FIG. 2. The local free energy for subcritical (solid line, $q=0.81$), critical (dashed line), and supercritical (dotted line, $q=0.85$) adhesion. The minimal adhesion threshold is given by $16(1-q_{cr})^2/q_{cr}^4=1$, which gives $q_{cr}=0.8284\ldots$. Two circles denote two stable phases [see Eq. (2)].

which describes the dynamics of phase separation with conserved order parameter (without proliferation), is the Cahn-Hilliard equation [13,14]. We now formulate the GCH equation by adding a proliferation term as follows:

$$\frac{\partial u}{\partial t}=\frac{\partial^2}{\partial x^2}\left(\ln(1-q)\frac{\partial^2 u}{\partial x^2}+\frac{df}{du}\right)+\alpha u(1-u), \tag{3}$$

where $u$ is the local density, $f$ is the local free energy, and $\alpha$ is the rate of proliferation. We write down the proliferation term $\alpha u(1-u)$ in the most common form, known as the *logistic growth* [15]. This form is widely used for modeling biological and ecological systems [15]. The proliferation term tends to zero both when there are no cells $(u=0)$ and when the density is maximal (all the sites are occupied, $u=1$). The gradient term in the total free energy functional is given by $(1/2)J(\partial u/\partial x)^2$, where $J$ represents interatomic interactions (for example, the coupling strength in the Ising model). This leads (in dimensionless form) to the $\partial^2/\partial x^2\times[-(J/kT)(\partial^2 u/\partial x^2)]$ term in Eq. (3). The mapping $q=1-\exp(-J/k_BT)$ explains the $\ln(1-q)$ coefficient in Eq. (3). Usually, the mean field form of the local free energy is assumed as follows:

$$f(u)=0.5a(u-0.5)^2+0.25b(u-0.5)^4. \tag{4}$$

Figure 2 shows the local free energy both for subcritical and supercritical adhesion. The only extremum (minimum) of $f(u)$ for subcritical adhesion is at $u=1/2$, so the homogeneous state is stable. For supercritical adhesion, the extremum at $u=1/2$ becomes a maximum, the homogeneous state is no longer stable, and two new minima appear, with the densities given by Eq. (2).

The constants $a$ and $b$ in Eq. (4) are chosen in such a way that the free energy functional satisfies several important conditions. First, we demand that the phase transition threshold is exact (and not its mean field approximation) as given by Eq. (2). Second, as the adhesion parameter $q$ tends to zero, $b$ should go to zero. Then Eq. (3) transforms into the FK equation. In addition, the diffusion coefficient in Eq. (1)

should be $\bar{D}=1/4$ (as can be derived from the discrete model without adhesion [7]), so that $\lim_{q\to 0} a=1/4$. We chose the following expressions:

$$a=-\frac{q-q_{cr}}{|q-q_{cr}|^{3/4}}\frac{c(q)}{4q_{cr}^{1/4}},$$

$$b=\left[\frac{q-q_{cr}}{1-16(1-q)^2/q^4}\right]^{1/4}\frac{c(q)}{q_{cr}^{1/4}}, \tag{5}$$

where the only restriction on the function $c(q)$ is that it should tend to unity when $q$ goes to zero. This function will be used to fit the continuum results with the results of discrete simulations. Note that the theoretical analysis is performed for the general form of local free energy and the specific relations (5) are used only when comparing theoretical predictions with numerical simulations. In the next section we consider the regime of subcritical adhesion and focus on front propagation.

## III. SUBCRITICAL ADHESION: FRONT PROPAGATION

### A. Theory

Initially, we put cells into the left part of the channel; $x$ measures the distance along the channel. In the initial state all sites with $x<0$ are occupied and the rest are empty. For $t>0$, cells diffuse and proliferate along the channel and form an advancing front. To analyze those fronts, we look for the solutions in the form $u=u(\xi=x-vt)$ in Eq. (3), where the front velocity $v$ is *unknown*. This gives

$$\ln(1-q)u''''+\frac{d^2f}{du^2}u''+\frac{d^3f}{du^3}u'^2+vu'+\alpha u(1-u)=0. \tag{6}$$

In order to understand velocity selection, we linearize Eq. (6) in the tail region $u=0$, in a similar way to the analysis of pulled fronts in the FK equation. Substituting $u\propto\exp(\lambda\xi)$, we find

$$E=\ln(1-q)\lambda^4+\left(\frac{d^2f}{du^2}\bigg|_{u=0}\right)\lambda^2+v\lambda+\alpha=0. \tag{7}$$

The behavior of the density front in the tail region depends on the sign of the determinant

$$D(v)=-\left(\frac{P^2}{9}+\frac{4r}{3}\right)^3+\left(-\frac{P^3}{27}+\frac{4Pr}{3}-\frac{Q^2}{2}\right)^2,$$

where

$$P=\left(\frac{d^2f}{du^2}\bigg|_{u=0}\right)\frac{1}{\ln(1-q)},$$

$$r=\frac{\alpha}{\ln(1-q)},$$

and

$$Q=\frac{v}{\ln(1-q)}.$$

As in the FK equation, there is an interval of possible velocities, $v>v_{\min}$. We checked numerically that for small enough

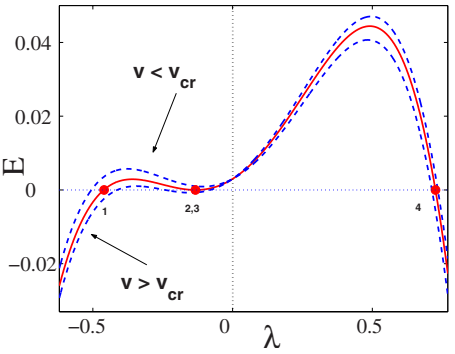


FIG. 3. (Color online) The characteristic equation $E$ [Eq. (7)] for different values of front velocity. The solid line corresponds to the critical velocity [given by Eq. (8)]. The two dashed lines correspond to larger and smaller velocities. The intersection of the horizontal dotted line $E=0$ with the solid line gives four roots of the characteristic equation (circles). The parameters are $q=0.4, \alpha=0.003$.

$\alpha$ [or small enough $q$ (see below)], velocity selection is determined by the condition $D=0$. This gives the minimum velocity of front propagation (the critical velocity) as follows:

$$v_{cr}^2=\frac{8\alpha}{3}\left(\frac{d^2f}{du^2}\bigg|_{u=0}\right)-\frac{2}{27\ln(1-q)}\left(\frac{d^2f}{du^2}\bigg|_{u=0}\right)^3 \times\left\{1-\left[1+12\alpha\ln(1-q)\left(\frac{d^2f}{du^2}\bigg|_{u=0}\right)^{-2}\right]^{3/2}\right\}. \tag{8}$$

As expected, $v_{cr}$ tends to zero when $\alpha$ goes to zero (fronts do not propagate for zero proliferation), and $v_{cr}$ tends to the value of the FK equation with $\bar{D}=1/4$ [see Eq. (1)], $v_{cr}\to\sqrt{\alpha}$, when the adhesion parameter $q$ goes to zero.

The selection rule is illustrated in Fig. 3. If the velocity is slightly larger than $v_{cr}$, Eq. (7) has four real roots: three negative and one positive. As the velocity approaches $v_{cr}$, two negative roots approach each other and coincide exactly when $D=0$ (see Fig. 3). It is reasonable to suppose, in view of the results for the FK equation, that this is the selected velocity of front propagation (see [16]). For smaller velocity these two roots become complex, which is not allowed as it results in an oscillatory behavior of the density in the tail region.

To test these predictions, we performed numerical simulations of Eq. (3). We used the third-order Runge-Kutta method, with a mesh size $\delta x=1.0$, and a time step $\delta t=0.03$. Initial conditions were localized: $u=0$ ahead of the front, $u=1$ behind the front, and the interface had the form $u=\exp(-x)/[1+\exp(-x)]$. Simulations confirm that the front velocity tends to the value given by Eq. (8). As in the FK equation, $v$ approaches $v_{cr}$ quite slowly (see Fig. 4).

Note that Eq. (8) becomes invalid when $\alpha$ (or $q$) are large enough, so that $1+12\alpha\ln(1-q)(d^2f/du^2|_{u=0})^{-2}$ becomes negative. In this case the characteristic equation (7) has two real roots [one negative ($\lambda_1$) and one positive ($\lambda_4$)] and two complex conjugate roots with a negative real part ($\lambda_{2,3}=\gamma\pm i\omega$). Therefore, the density in the tail region is oscillatory and becomes negative, which is forbidden. This is an

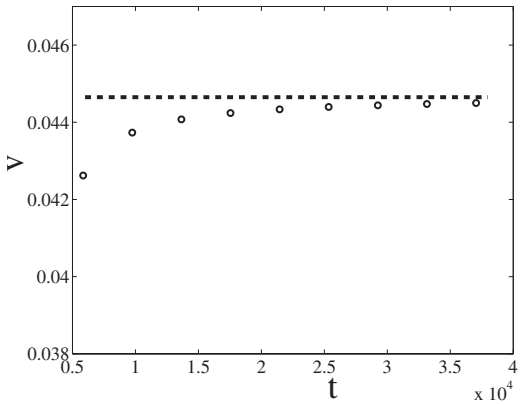


FIG. 4. Front velocity from the numerical solution of Eq. (3) as a function of time (circles). The velocity slowly approaches the theoretical value (dashed line), similar to the situation in the FK equation. The parameters are $q=0.6$ and $\alpha=0.003$.

inherent feature of the time-dependent equation (3). It is known that solutions of fourth-order differential equations generally do not remain positive [17]. A similar effect occurs in the extended Fisher-Kolmogorov equation (EFK) [16]. It was shown that in some region of parameters localized initial conditions cannot develop into a uniformly translating front solution. Instead, for sufficiently sharp initial conditions one has an *envelope front*: a moving front creates a periodic array of kinks behind it [16]. These oscillations between $u=1$ and $u=-1$ occur due to the cubic nonlinearity in the reaction term of the EFK equation. In our case, $u=-1$ is not a fixed point, so negative perturbations are not stabilized [in fact, numerical simulations of Eq. (3) show a finite-time explosion in this region of parameters.] In addition, $u<0$ has no physical meaning in our case. A possible way to overcome this problem is to demand $u\geq 0$ when solving Eq. (3). In this case, the density profile is not analytic, as in problems with compact support: the density becomes zero at some $\xi_{crit}$ and remains zero for $\xi>\xi_{crit}$. This profile propagates with a well defined velocity (see Fig. 5). We believe that this is the only type of solution that can be chosen in this regime.

### B. Comparison with discrete simulations

Now we compare the results of the deterministic continuum approach with stochastic discrete modeling. Figure 5 shows the front velocity as a function of the adhesion parameter $q$ for different values of proliferation, $\alpha$. The theoretical predictions are given by Eq. (8). The front velocity in the discrete system is obtained by averaging over many realizations. One can see excellent agreement over a wide range of parameters. [Front velocity computed numerically from Eq. (3) also approaches the same values (see Fig. 4)]. The theoretical curve corresponding to large $\alpha$ becomes invalid for large $q$, which is related to the oscillatory behavior of density tails. Nevertheless, the numerically calculated front velocities in this region are well defined and agree with those from discrete simulations. This shows that our theoretical understanding in this case is incomplete.

Figure 6 shows an example of the corresponding density profiles from discrete and continuum simulations. The form

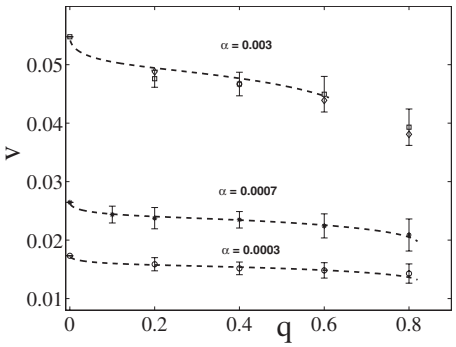


FIG. 5. Front velocity as a function of the adhesion parameter $q$ for different values of proliferation $\alpha$. The theoretical predictions are given by Eq. (8) (dashed lines). The front velocity in the discrete system is obtained by averaging over many realizations. The calculations in Eq. (8) were performed for $c(q)=1-0.75q^{1/2}$ in the expression for free energy, which gives the best agreement with discrete simulations. One can see that the theoretical curve corresponding to large $\alpha$ becomes invalid for large $q$, which is related to the oscillatory behavior of density tails. Nevertheless, the numerically calculated front velocities in this region are well defined and agree with those from discrete simulations. Front velocities computed from the time-dependent equation (3) are shown by diamonds. The values of proliferation are $\alpha=0.0003$ (circles), $\alpha=0.0007$ (asterisks), and $\alpha=0.003$ (squares).

of the fronts is very similar, and discrete and continuum fronts propagate with the same velocity. Note, however, that the transient regime for the discrete front is longer.

## IV. SUPERCRITICAL ADHESION

The situation for $q>q_c$ is more complicated. As before, we start with a sharp front: $u=1$ for $x<0$ and $u=0$ for $x>0$. It turns out there is a nontrivial and long-lived transient behavior [1], which we analyze using discrete and continuum approaches.

### A. Nonzero proliferation

We first consider $\alpha\neq 0$, $q>q_c$. Figure 7 shows a time series of density profiles. To obtain the profiles, we averaged

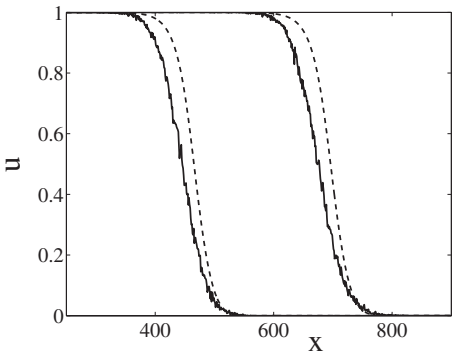


FIG. 6. Time series of density profiles in discrete (solid lines) and continuum (dashed lines) models. The parameters are $q=0.4$ and $\alpha=0.003$. The discrete fronts correspond to times $t_{d1}=10\,000$ (the left curve) and $t_{d2}=15\,000$ (the right curve); the density profiles computed from the numerical solution of Eq. (3) correspond to times $t_{c1}=6000$ (the left curve) and $t_{c2}=11\,000$ (the right curve).

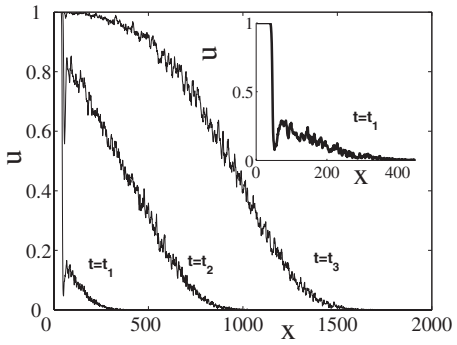


FIG. 7. Time series of density profiles in discrete simulations. The inset shows a magnified picture of the density profile for early time $t=t_1$. The parameters are $q=0.9$, $\alpha=0.0003$, $t_1=2.2\times10^4$, $t_2=6.6\times10^4$, and $t_3=11\times10^4$.

the density over the channel width and over many realizations. One realization is shown in Fig. 8. A long-lived transient occurs before the propagating front is formed. The inset in Fig. 7 shows a magnified picture of the density profile for early time. An interesting feature is the secondary density peak. This peak occurs due to phase separation and cluster formation in the low-density invasive region. At later times the main front builds up and catches the isolated clusters. The same feature is present in the continuum approach: Fig. 9 shows a time series of density profiles from numerical solutions of Eq. (3).

The transient behavior with a secondary density peak occurs due to the slow (nonexponential) decay of the tail, which occurs only for supercritical adhesion. For $\alpha>0$, there are two competing processes: the (slow) propagation of the front and relatively fast formation of the secondary peak on the slowly decaying tail. This slowly decaying tail also exists for zero proliferation. In order to gain some insight into its formation, we now study the relaxation dynamics in a Cahn-Hilliard equation [Eq. (3)] without proliferation.

### B. Zero proliferation

In this section we focus on the relaxation dynamics (for zero proliferation) both in the discrete and continuum models. We start with the discrete lattice model. Initially, all channel sites with $x<0$ are occupied ($u=1$), and sites with $x>0$ are empty ($u=0$). However, since $q>q_c$, the final state consists of two phases: a high-density phase $u=u_1(q)$ for $x<0$ and a low-density phase $u=u_2(q)$ for $x>0$ [see Eq. (2)].

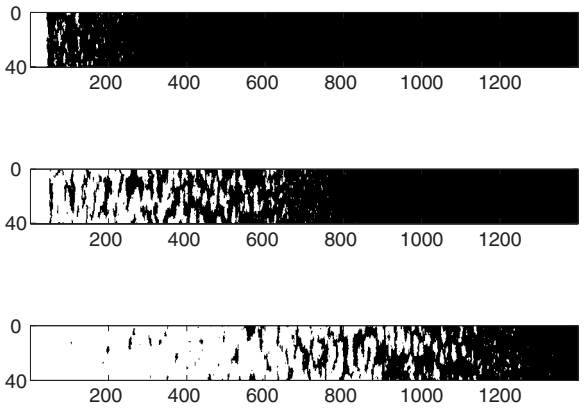

FIG. 8. Time series of snapshots, corresponding to the density profiles in Fig. 7. The upper panel corresponds to $t_1=2.2\times10^4$, the middle panel to $t_2=6.6\times10^4$, and the lower panel to $t_3=11\times10^4$. The parameters are the same as in Fig. 7.

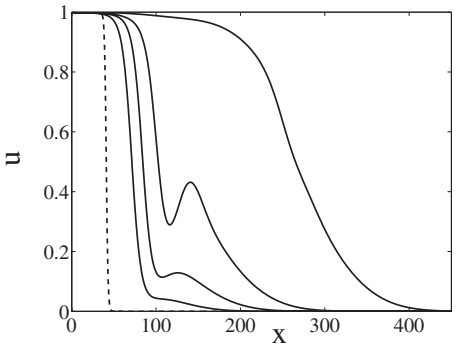


FIG. 9. Time series of density profiles from the numerical solution of Eq. (3). The parameters are $q=0.9$, $\alpha=0.0003$, $t_0=0$ (dashed line), $t_1=1.8\times10^4$, $t_2=2.4\times10^4$, $t_3=3.0\times10^4$, and $t_4=4.4\times10^4$ (curves from left to right, solid lines).

Figure 10 shows the tails of two density profiles calculated from the discrete model. As before, we averaged over the channel width and over many realizations. The relaxation dynamics is self-similar. The inset shows that the same density tails coincide when measured as a function of $\eta=x/\sqrt{t}$, as expected for purely diffusive behavior.

The same relaxation dynamics occurs in the continuum model. This behavior can be easily explained. Considering the small-density region (the tail), we can neglect the $\ln(1-q)(\partial^2 u/\partial x^2)$ term in Eq. (3). Then, substituting $u=u(\eta)$ into Eq. (3), we have

$$\left(\frac{d^2 f}{du^2}\right) + \frac{1}{2}\eta u' = 0, \tag{9}$$

where $'$ is the derivative with respect to $\eta$. To solve this equation we need to specify two boundary conditions at $\eta=0$. The first one is just $u(\eta=0)=u_2$ (the low-density stable

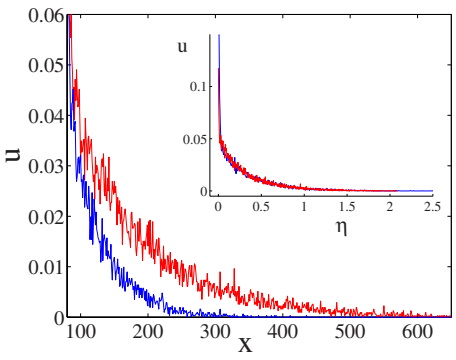


FIG. 10. (Color online) Density profiles (tails) for different times as computed from the discrete model. The inset shows the same density tails as a function of $\eta=x/\sqrt{t}$. The parameters are $q=0.85$, $t_1=2\times10^4$ (the left curve), and $t_2=10^5$ (the right curve).

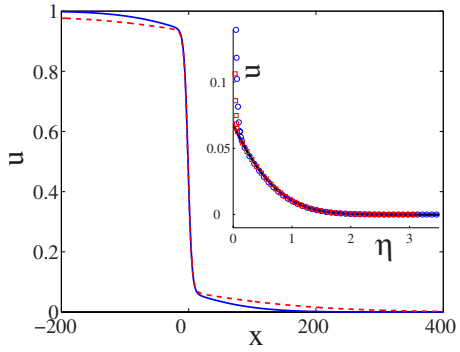


FIG. 11. (Color online) Density profiles for different times (blue solid curve at $t_1=1.5\times10^4$; red dashed curve at $t_2=6\times10^4$) as computed from Eq. (3). The inset shows that the tails of density profiles corresponding to different times coincide when measured as a function of $\eta=x/\sqrt{t}$. The blue circles correspond to $t_1$; the red squares correspond to $t_2$. The asymptotics computed from Eq. (9) are shown by the solid black line. The adhesion parameter is $q=0.85$. The simulations were performed for $c=4q_c^{1/4}$ in the expression for free energy.

phase). Then we find $u'(\eta=0)$ by a shooting procedure, demanding $u(\eta\to\infty)\to0$.

Figure 11 shows this self-similar relaxation dynamics. Two density profiles depicted in Fig. 11 are calculated from the time-dependent equation (3). The inset shows that these profiles (the tails), corresponding to different times, coincide when measured as a function of $\eta=x/\sqrt{t}$. The asymptotics computed from Eq. (9) is in excellent agreement with numerical simulations.

Correlations to the purely diffusive behavior may arise in the discrete model due to effects of cell-cell adhesion. However, these effects are negligibly small when the density is very low. Therefore, we observe a purely diffusive behavior in the tail region both in the continuum and discrete models. The discrepancies between the results of simulations of continuum and discrete models (see Figs. 10 and 11) are due to the fact that the "true" free energy is unknown.

This self-similar behavior means that the decay rate is inversely proportional to $t^{1/2}$, so it becomes lower with time. This is the base of the formation of a secondary density peak in the transient regime for nonzero proliferation.

## V. SUMMARY AND DISCUSSION

In this work we formulated and examined a continuum model for motile and proliferative cells, which experience cell-cell adhesion. We described collective behavior of the cells by using a modified Cahn-Hilliard equation with an additional proliferation term. We identified and analyzed different parameter regimes: front propagation for subcritical adhesion, nontrivial transient regime for supercritical adhesion, and nonzero proliferation. The results of the continuum description in various regimes are compared with the results of a discrete model [1].

The continuum approach we used is phenomenological. It is presently unknown how to proceed from the microscopic lattice model to a macroscopic continuum description even without proliferation (for zero proliferation this is model B of dynamic critical phenomena). One way is to use the mean field approximation [14], which neglects fluctuations. However, even the statics, namely, the phase diagram, Fig. 1, in the mean field approximation is very different from the exact solution. We have taken another approach, choosing the free energy functional that includes exact statics in it. This allows us to compare the results of continuum simulations with the results of the discrete model.

The results of continuum theory are in qualitative agreement with discrete simulations in a wide region of parameters, in particular, for the velocity of front propagation in the subcritical regime. The continuum approach reproduced a secondary density peak formation in the transient regime. However, there are important quantitative differences. Discrete simulations show that the high-density part of the profile diffuses much more slowly than the low-density part. At later times this leads to much smoother fronts than in the continuum simulations. There is no symmetry between particles and holes (occupied and empty sites) in the discrete model [14]. We could introduce a density-dependent mobility to take this effect into account in the continuum description. For example, one can consider the following expression for mobility: $M=1-qu^2$, or similar forms where $M$ is a decreasing function of density [18].

The modified Cahn-Hilliard equation admits solutions in the form of propagating fronts. We postulated that the velocity selection procedure is similar to that of the FK equation and found a critical velocity, Eq. (8). Numerical simulations of the time-dependent equation (3) confirmed this result. However, the expression for critical velocity becomes invalid in some region of parameters. Nevertheless, demanding $u\geq0$ we can still solve Eq. (3) numerically and observe propagating fronts with a well-defined velocity (see Fig. 5). This problem still needs to be clarified.

An interesting avenue of future work is applying the modified Cahn-Hilliard equation to the problem of cluster nucleation and growth in a two-dimensional system to model clustering of malignant brain tumor cells.

## ACKNOWLEDGMENTS

We thank P. Smereka and J. Lowengrub for useful discussions and the NIH Bioengineering Research Partnership grant (Grant No. R01 CA085139-01A2) for support.

[1] E. Khain, L. M. Sander, and C. M. Schneider-Mizell, J. Stat. Phys. **128**, 209 (2007).

[2] D. Drasdo, R. Kree, and J. S. McCaskill, Phys. Rev. E **52**, 6635 (1995); J. A. Sherratt and J. C. Dallon, C. R. Biologies **325**, 557 (2002); P. K. Maini, D. L. S. McElwain, and D. Leavesley, Appl. Math. Lett. **17**, 575 (2004).

[3] J. A. Sherratt and M. A. J. Chaplain, J. Math. Biol. **43**, 291 (2001); L. M. Sander and T. S. Deisboeck, Phys. Rev. E **66**, 051901 (2002); K. R. Swanson, C. Bridge, J. D. Murray, and E. C. Alvord, J. Neurol. Sci. **216**, 1 (2003); H. Hatzikirou, A. Deutsch, C. Schaller, M. Simon, and K. Swanson, Math. Models Meth. Appl. Sci. **15**, 1779 (2005); C. Athale, Y. Mansury, and T. S. Deisboeck, J. Theor. Biol. **233**, 469 (2005); E. Khain, L. M. Sander, and A. Stein, Complexity **11**, 53 (2005); E. Khain and L. M. Sander, Phys. Rev. Lett. **96**, 188103 (2006); P. Macklin and J. Lowengrub, J. Math. Biol. **245**, 677 (2007); S. Fedotov and A. Iomin, Phys. Rev. Lett. **98**, 118101 (2007); P. Gerlee and A. R. A. Anderson, Phys. Rev. E **75**, 051911 (2007); M. J. Simpson, A. Merrifield, K. A. Landman, and B. D. Hughes, *ibid.* **76**, 021918 (2007); S. Fedotov and A. Iomin, *ibid.* **77**, 031911 (2008).

[4] S. Turner, J. A. Sherratt, K. J. Painter, and N. J. Savill, Phys. Rev. E **69**, 021910 (2004); S. Turner, *ibid.* **71**, 041903 (2005).

[5] M. Bramson, P. Calderoni, A. Demasi, P. Ferrari, J. Lebowitz, and R. H. Schonmann, J. Stat. Phys. **45**, 905 (1986); A. R. Kerstein, *ibid.* **45**, 921 (1986).

[6] E. Brunet and B. Derrida, Phys. Rev. E **56**, 2597 (1997); D. A. Kessler, Z. Ner, and L. M. Sander, *ibid.* **58**, 107 (1998); E. Brunet and B. Derrida, J. Stat. Phys. **103**, 269 (2001); E. Moro, Phys. Rev. Lett. **87**, 238303 (2001); D. Panja, G. Tripathy, and W. van Saarloos, Phys. Rev. E **67**, 046206 (2003); E. Moro, *ibid.* **68**, 025102(R) (2003); D. Panja, Phys. Rep. **393**, 87 (2004).

[7] T. Callaghan, E. Khain, L. M. Sander, and R. M. Ziff, J. Stat. Phys. **122**, 909 (2006).

[8] R. A. Fisher, Proc. Annu. Symp. Eugen. Soc. **7**, 355 (1937); A. Kolmogorov, I. Petrovsky, and N. Piscounov, Moscow Univ. Bull. Math. **1**, 1 (1937).

[9] Note, however, that the front velocity in the discrete system is smaller than its continuum analog and approaches it extremely slowly [6,7].

[10] D. G. Aronson and H. F. Weinberger, Adv. Math. **30**, 33 (1978).

[11] L. Onsager, Phys. Rev. **65**, 117 (1944).

[12] K. Huang, *Statistical Mechanics* (Wiley, New York, 1987).

[13] J. S. Langer, in *Solids Far from Equilibrium*, edited by C. Godreche (Cambridge University Press, Cambridge/New York, 1992), pp. 297–364.

[14] J. F. Gouyet, M. Plapp, W. Dieterich, and P. Maass, Adv. Phys. **52**, 523 (2003); M. Plapp and J. F. Gouyet, Phys. Rev. E **55**, 5321 (1997).

[15] J. D. Murray, *Mathematical Biology* (Springer, New York, 2002).

[16] W. van Saarloos, Phys. Rev. Lett. **58**, 2571 (1987); W. van Saarloos, Phys. Rev. A **37**, 211 (1988); G. T. Dee and W. van Saarloos, Phys. Rev. Lett. **60**, 2641 (1988); W. van Saarloos, Phys. Rev. A **39**, 6367 (1989).

[17] P. Smereka (private communication).

[18] J. S. Langer, M. Bar-on, and H. D. Miller, Phys. Rev. A **11**, 1417 (1975); K. Kitahara and M. Imada, Suppl. Prog. Theor. Phys. **64**, 65 (1978); S. Puri, A. J. Bray, and J. L. Lebowitz, Phys. Rev. E **56**, 758 (1997).